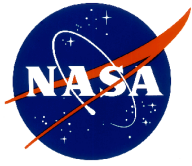


JPL Document D-94249



Exoplanet Exploration Program Technology Plan

Appendix: 2015

Peter Lawson with revisions by Nick Siegler and Brian Lim

**National Aeronautics and
Space Administration**

**Jet Propulsion Laboratory
California Institute of Technology
Pasadena, California**

20 January 2015

This research was carried out at the Jet Propulsion Laboratory, California Institute of Technology, under a contract with the National Aeronautics and Space Administration.

Reference herein to any specific commercial product, process, or service by trade name, trademark, manufacturer, or otherwise, does not constitute or imply its endorsement by the United States Government, or the Jet Propulsion Laboratory, California Institute of Technology.

© 2015 California Institute of Technology. Government Sponsorship acknowledged.

Approvals

Released by

Nick Siegler, Exoplanet Exploration Program Technology Manager, JPL

Approved by

Gary Blackwood, Exoplanet Exploration Program Manager, JPL

Douglas Hudgins, Exoplanet Exploration Program Scientist, NASA HQ

John Gagosian, Exoplanet Exploration Program Executive, NASA HQ

Contents

| | |
|---|------------|
| APPROVALS..... | III |
| CONTENTS | IV |
| APPENDIX A EXOPLANET TECHNOLOGY OBJECTIVES | 5 |
| A.1 INTRODUCTION..... | 5 |
| A.1.1 Program Goals..... | 5 |
| A.1.2 Coronagraph and Starshade STD T..... | 6 |
| A.1.3 Previously Funded Efforts..... | 7 |
| A.2 WFIRST/AFTA AND CORONAGRAPH SYSTEM TECHNOLOGY | 10 |
| A.2.1 Low-order Wavefront Sensing & Control..... | 10 |
| A.2.2 Large Format, Ultra-low Noise Visible Detectors | 10 |
| A.2.3 Deformable Mirror Technology | 10 |
| A.2.4 Efficient Contrast Convergence..... | 11 |
| A.3 CORONAGRAPH TECHNOLOGY REQUIREMENTS | 13 |
| A.3.1 Specialized Coronagraph Optics..... | 13 |
| A.3.2 MEMS Deformable Mirror Technology..... | 18 |
| A.3.3 Other Coronagraph Technologies..... | 19 |
| A.4 STARSHADE TECHNOLOGY REQUIREMENTS | 20 |
| A.4.1 Control of Scattered Sunlight..... | 21 |
| A.4.2 Validation of Starshade Optical Models..... | 21 |
| A.4.3 Lateral Formation Flying Sensing Accuracy..... | 22 |
| A.4.4 Flight-Like Petal Fabrication and Deployment..... | 23 |
| A.4.5 Inner Disk Deployment | 24 |
| A.4.6 Other Starshade Technologies..... | 25 |
| A.5 CONCLUSION | 25 |
| A.6 BIBLIOGRAPHY..... | 26 |

Appendix A

Exoplanet Technology Objectives

A.1 Introduction

The purpose of this Appendix is to guide near-term (1–5 year) technology development for future space observatories related to NASA's Exoplanet Exploration Program (ExEP). A long-term goal of the Program is a *New Worlds Mission*, such as that envisaged by the 2010 Astronomy and Astrophysics Decadal Survey [1] - a mission capable of directly imaging terrestrial planets in the habitable zones of stars in the Solar neighborhood, and measuring their spectra to search for the telltale signs of life. Such a mission will require extreme starlight suppression and new technology developments will be needed to achieve the extreme degree of contrast that will be required.

Through this work it should also be possible in the near term to enable other missions whose science is compelling and essential to understanding the birth and evolution of planetary systems and the conditions that lead to life in the Universe.

The subjects covered here are those most directly relevant to recommendations in the 2010 Decadal Survey, with regard to a *New Worlds Technology Development Program* and a future *New Worlds Mission*. The greatest emphasis is therefore placed on starlight-suppression technology to enable the detection of Earth-like planets around Sun-like stars.

The necessary technology developments and ongoing activities are summarized in this Appendix. An excellent overview of the challenges of direct imaging can be found in the volume *Exoplanets*, edited by S. Seager [2]. The interested reader will find additional details concerning exoplanet technology in the SPIE Conference Series on *Techniques and Instrumentation for the Detection of Exoplanets*, the most recent being Proc. SPIE vol. 8864.

A.1.1 Program Goals

The 2010 Decadal Survey recommended the creation of a *New Worlds Technology Development Program* to advance the technological readiness of the three primary starlight suppression architectures: coronagraphs, starshades, and interferometers. The Survey further recommended—if the scientific groundwork and design requirements were sufficiently clear—that an architecture downselect should be made in time for consideration by the 2020 Decadal Survey, and a significantly increased technology investment over the latter half of the decade should be focused to prepare a mission concept based on this architecture for consideration by the 2020 Survey.

“Thus the plan for the coming decade is to perform the necessary target reconnaissance surveys to inform next-generation missions while simultaneously completing the technology development to bring the goals within reach.” (NWNH, p. 39)

In response to the survey recommendations, the NASA *Astrophysics Implementation Plan (2014 Update)* describes a path leading to the selection of the next strategic mission after the James Webb Space Telescope. While emphasizing the priority of the Wide-Field Infrared Survey Telescope (WFIRST), the plan includes studies for exoplanet probe-scale missions as possible alternatives.

In support of this effort an implementation of WFIRST is being studied that uses a 2.4-m telescope of the Astrophysics Focused Telescope Assets (AFTA) that was donated to NASA. A high-contrast exoplanet coronagraph is also being studied as a second instrument for this mission. AFTA coronagraph technology is the subject of a separate technology plan developed by the AFTA Study Office and published in early 2014. That technology plan is advancing many of the coronagraph technology needs called out in this Plan. Consequently, the technology described in this document is devoted to instrument performance on missions capable of directly imaging and characterizing Earth-like planets such as recent probe-scale missions and future (non-AFTA) NWNH missions.

NASA's ExEP supports activities that contribute to the advancement of these exoplanet mission concepts. The Program funds and facilitates experiments and analyses selected by NASA HQ through yearly solicitations issued through the NASA omnibus Research Opportunities in Space and Earth Sciences (ROSES). The Program also provides support in the form of infrastructure, expertise, and test facilities to selected Principal Investigators.

As a part of ROSES, NASA currently funds technology development through the Astrophysics Research and Analysis (APRA) solicitation and the Technology Development for Exoplanet Missions (TDEM) component of the Strategic Astrophysics Technology (SAT) solicitation. APRA covers low-TRL technology research while SAT-TDEM covers maturation of mid-range TRL technologies. This two-stage approach supports the advancement of technology envisaged by the 2010 Decadal Survey. TDEM tasks funded for the 2009, 2010, 2012, and 2013 solicitations are listed in Tables A.1 and A.2.

The goal of exoplanet technology development is to enable future missions by demonstrating selected key technologies. This effort must include the establishment of performance error budgets tied to flight requirements and experimental demonstrations that the error budgets, or key components of the error budgets, can be met. Furthermore, models must be validated that demonstrate that the physics of the limiting error sources in those experiments are understood well enough to reliably predict the performance of the flight mission.

The recommendation by the 2010 Decadal Survey was to continue to pursue the development of coronagraph, external occulter, and interferometer technologies to allow an architecture downselect by the late-decade. Nevertheless, for both cost and technical readiness reasons, infrared interferometry is currently of lower priority as the basis for a *New Worlds Mission* than either of the coronagraph or starshade architectures.

A.1.2 Coronagraph and Starshade STDT

The NASA *Astrophysics Implementation Plan (2014 Update)* includes studies for exoplanet probe-scale missions as possible alternatives to a WFIRST/AFTA mission. The external occulter mission concept study is entitled Exo-S; the coronagraph mission concept study is

entitled Exo-C. Both Science and Technology Definition Teams' (STDT) 2014 Interim Reports can be found at <http://exep.jpl.nasa.gov/stdt/>. The Exo-S study will also include a scenario of flying a Starshade spacecraft with a WFIRST/AFTA mission. Their Final Reports will be made publicly available at the same website in early 2015. These reports will include detailed observatory and mission designs as well as an independent list of technology gaps and priorities.

A.1.3 Previously Funded Efforts

Tables A.1 and A.2 list the previously funded TDEM awards, grouped by research area. The results of these efforts are described in the text in Sections A.3 and A.4. Final reports for completed TDEMs as well as Milestone Whitepaper Reports for those still in process can be found at <http://exep.jpl.nasa.gov/technology/>.

Table 1. Starlight suppression technology research funded through the TDEM component of NASA's solicitation on SAT. Awards for calls from 2009, 2010, 2012, and 2013 are listed. Each award nominally provides two years of funding although more years can be proposed as well.

| Year | PI | Institution | Proposal Title |
|--|----------------|------------------|---|
| CORONAGRAPH STARLIGHT-SUPPRESSION DEMONSTRATIONS | | | |
| 2009 | John Trauger | JPL/Caltech | Advanced Hybrid Lyot Coronagraph Technology for Exoplanet Missions |
| 2010 | Eugene Serabyn | JPL/Caltech | Demonstrations of Deep Starlight Rejection with a Vortex Coronagraph |
| 2009 | Olivier Guyon | Univ. of Arizona | Phase-Induced Amplitude Apodization Coronagraphy Development and Laboratory Validation |
| 2010 | Olivier Guyon | Univ. of Arizona | Advances in Pupil Remapping (PIAA) coronagraphy: improving Bandwidth, Throughput and Inner Working Angle |
| 2009 | Mark Clampin | NASA/GSFC | Visible Nulling Coronagraph Technology Maturation: High Contrast Imaging and Characterization of Exoplanets |
| 2010 | Richard Lyon | NASA/GSFC | Compact Achromatic Visible Nulling Coronagraph Technology Maturation |
| 2013 | Richard Lyon | NASA/GSFC | Segment Aperture Nulling Coronagraphy |
| 2010 | Jagmit Sandhu | JPL/Caltech | Visible Nulling Coronagraph (VNC) Technology Demonstration Program |

| Year | PI | Institution | Proposal Title |
|---|------------------|------------------------------------|---|
| STARSHADE STARLIGHT-SUPPRESSION DEMONSTRATIONS | | | |
| 2009 | N. Jeremy Kasdin | Princeton University | Starshades for Exoplanet Imaging and Characterization: Key Technology Development |
| 2010 | N. Jeremy Kasdin | Princeton University | Verifying Deployment Tolerances of an External Occulter for Starlight Suppression |
| 2012 | N. Jeremy Kasdin | Princeton University | Optical and Mechanical Verification of an External Occulter for Straight Suppression |
| 2013 | N. Jeremy Kasdin | Princeton University | Formation Flying for External Occulters |
| 2012 | Suzanne Casement | Northrop Grumman Aerospace Systems | Starshade Stray Light Mitigation through Edge Scatter Modeling and Sharp-Edge Materials Development |
| 2012 | Tiffany Glassman | Northrop Grumman Aerospace Systems | Demonstration of Starshade Starlight-Suppression Performance in the Field |
| 2013 | Webster Cash | University of Colorado | Development of Formation Flying Sensors |

Table A.2 Supporting technology research funded through the TDEM component of NASA's solicitation on SAT.

| Year | PI | Institution | Proposal Title |
|---|--------------------|----------------------------------|--|
| WAVEFRONT SENSING & CONTROL OF SCATTERED STARLIGHT | | | |
| 2009 | Martin Noecker | Ball Aerospace | Advanced Speckle Sensing for Internal Coronagraphs and Methods of Isolating Exoplanets from Speckles |
| 2010 | N. Jeremy Kasdin | Princeton University | Integrated Coronagraph Design and Wavefront Control using Two Deformable Mirrors |
| 2010 | Paul Bierden | Boston Micromachines Corporation | MEMS Deformable Mirror Technology Development for Space-Based Exoplanet Detection |
| 2010 | Michael Helmbrecht | Iris AO | Environmental Testing of MEMS Deformable Mirrors for Exoplanet Detection |
| 2009 | John Krist | JPL/Caltech | Assessing the Performance Limits of Internal Coronagraphs Through End-to-End Modeling |

| | | | |
|-------------|-------------------|-------------|--|
| 2010 | Stuart Shaklan | JPL/Caltech | Coronagraph Starlight Suppression Model Validation: Coronagraph Milestone #3A |
|-------------|-------------------|-------------|--|

| Year | PI | Institution | Proposal Title |
|-------------|-----------|--------------------|-----------------------|
|-------------|-----------|--------------------|-----------------------|

OTHER TECHNOLOGIES

| | | | |
|-------------|--------------|-----------------------|---|
| 2009 | Donald Figer | Rochester Inst. Tech. | A Photon-Counting Detector for Exoplanet Missions |
|-------------|--------------|-----------------------|---|

| | | | |
|-------------|-------------------|------------------------------|--|
| 2013 | Eduardo Bendek | NASA Ames Research Center | Enhanced Direct Imaging Exoplanet Detection with Astrometric Mass Determination |
|-------------|-------------------|------------------------------|--|

A.2 WFIRST/AFTA and Coronagraph System Technology

The following subsections are included here to highlight areas of planned WFIRST/AFTA technology development that would also be supportive of other coronagraph concepts.

The main starlight suppression challenges of the WFIRST/AFTA coronagraph are due to the fact that its telescope was never designed for coronagraphy. It uses an input pupil that is obscured by a large secondary mirror, which in turn is supported by six struts. This introduces complex diffraction features that are absent in designs that use unobscured pupils. Consequently, the masks and selected input optics will require technology development that is specific to WFIRST/AFTA. Nonetheless, demonstrations of WFIRST/AFTA technology will require augmentations and improvements to other technologies and testbed infrastructure that may be made available to test other concepts. A non-exhaustive list of technologies to be developed by WFIRST/AFTA is described here. Technology development for the WFIRST/AFTA coronagraph is the subject of a separate technology plan developed by the AFTA Study Office early in 2014.

A.2.1 Low-order Wavefront Sensing & Control

A slight misalignment or deformation of the incident starlight wavefront to the coronagraph could cause scattered light to appear within the dark hole of the coronagraph that could obscure or even mimic the presence of a planet. It is therefore important to validate the design of a suitable pointing and low-order control system for a coronagraph. This system would have to be integrated with the control of the body pointing of the spacecraft.

A first step in this direction was accomplished with the development of the Phase-Induced Amplitude Apodization coronagraph system in the High Contrast Imaging Testbed (HCIT) 2 testbed. Sub-milliarcsecond pointing stability was demonstrated in vacuum with a servo system, with the intent of eventually expanding it to demonstrate low-order wavefront sensing and control [26].

A low-order wavefront sensor uses the bright starlight that is rejected by the coronagraph and measures not only pointing changes but low-order aberrations such as defocus, coma, and spherical aberration. Static and dynamic low-order wavefront errors are anticipated due to slight imperfections in the optical design and thermally induced mechanical distortions of the optics that might be experienced in flight. The corrections of low-order wavefront errors—other than pointing—has not yet been demonstrated and is a priority of the WFIRST/AFTA technology development program. They have selected as their baseline a Zernike wavefront sensor and integrated demonstrations with a coronagraph in the HCIT are planned for mid-2015.

A.2.2 Large-Format, Ultra-Low Noise Visible Detectors

The WFIRST/AFTA coronagraph will need high-performance ultra-low-light level visible detectors for use in its science camera and its integral field spectrograph. Advances are needed in the achievable noise performance and in particular the quantum efficiency achievable in the wavelength range of 0.9–1.0 μm . There are several options, notably the Electron-Multiplying CCDs (EMCCDs) manufactured by e2v. The WFIRST/AFTA coronagraph technology development effort has baselined the e2v CCD201 detector (1024 x 1024; 13 μm x 13 μm pixel size) and includes characterization and radiation testing. In

2014 e2V developed its first 4kx4k EMCCD and is being characterized by an initial set of customers.

The only detector technology work funded through the TDEM program has been Donald Figer (Rochester Institute of Technology) to raise the technology readiness of Avalanche Photodiode (APD) arrays. A Final Report was approved by the Program in 2014 [74].

This effort was a demonstration of new detector technology that may greatly improve the science throughput of coronagraph and starshade mission concepts due to ultra-low read-out noise. A silicon 256x256 diode array was bonded to a Read Out Integrated Circuit (ROIC); the array had been hybridized and tested [75]; and a first-light image had been obtained. This device has a 100% fill factor and a good response from 300–1000 nm. Radiation tests have been completed. While this work was completed in 2014, only 3 of the 5 success criteria were met. Future work in this area may include the performance validation of silicon focal plane arrays with a larger number of pixels (1024x1024 vs 256x256).

A.2.3 Deformable Mirror Technology

Wavefront aberrations less than $1/10,000^{\text{th}}$ of a wave must be maintained in a coronagraph if contrasts of 1×10^{-10} contrast are to be achieved. At visible wavelengths, this implies wavefront control at the level of angstroms, and deformable mirror (DM) technology is therefore required to compensate for residual optical aberrations.

Two DMs are required to create a symmetric dark hole around the image of a star, correcting both amplitude and phase errors across the full available field of view. The standard practice in lab experiments up until 2013 has been to use only a single DM and create a half dark-hole, offset to one side of the star.

The WFIRST/AFTA coronagraph will use two 48x48 element electrostrictive lead magnesium niobate (PMN) DMs made by AOA Xinetics. These mirrors represent the state of the art and are routinely used in the HCIT vacuum testbeds. They have produced all the reported results of contrasts better than 1×10^{-9} . One Xinetics PMN-based DM has already been successfully vibration tested at JPL.

The DMs for the AFTA coronagraph will be implemented in the testbeds in a flight-like configuration: there will be a pair of DMs in the beam path prior to the starlight suppression optics, controlled to create a dark hole that is symmetric about the star.

Jeremy Kasdin (Princeton University) and collaborators were funded through a 2010 TDEM award to demonstrate 2-DM wavefront control using a Shaped Pupil Coronagraph. Their goal was to achieve better than 1×10^{-9} raw contrast at 10% bandwidth. Raw contrasts of 3.6×10^{-9} were achieved using an optical configuration that was not optimized for the demonstrations (due to scheduling constraints).

A.2.4 Efficient Contrast Convergence

High-order focal-plane wavefront sensing is accomplished by modulating the input wavefronts using one or more deformable mirrors and measuring phase and amplitude changes in speckles at the science camera. This technique removes the non-common-path error induced by using a separate sensor. The sensing is accomplished at the detector using the photons collected there by the coronagraph, and it is desirable to minimize the time spent correcting the wavefront to create a “dark hole” where the planet can be detected.

Currently, high-contrast wavefront correction schemes are semi-empirical: they combine independent measurements of masks, static wavefronts, and DMs with Fourier and Fresnel models of their interactions and a nulling algorithm such as electric field conjugation to predict how DM motions will affect contrast and to produce corrections that minimize it. Model and measurement uncertainties limit the rate of wavefront control convergence at contrasts better than 10^{-8} , requiring many iterations to reach contrasts on the order of 10^{-10} . Typical numbers of iterations to converge to 10^{-10} contrast are on the order of many tens to hundreds.

We require efficient methods to improve this rate of convergence, such that the contrast floor of a coronagraph capable of contrast better than 10^{-10} may be reached in a few iterations (better than 10-20 starting from a flat DM setting). These may include nulling algorithms that are more tolerant to uncertainties in component-level characterization and methods to efficiently calibrate the effects of DM motions at high contrasts. Methods usable in broadband light (10% or better) and at small inner working angles are particularly sought after.

A.3 Coronagraph Technology Requirements

A.3.1 Specialized Coronagraph Optics

A continuing program to advance the performance of masks, apodizers, or beam-shaping optics to better than AFTA coronagraph performance requirements is yet needed. This should include improved designs to improve inner working angle ($< 3 \lambda/D$), contrast performance ($\leq 10^{-10}$), bandwidth ($\geq 10\%$), and throughput. Demonstrated results in this area are summarized by Lawson et al. (2013) and are described below and illustrated in Figs. A.1 and A.2.

There are several approaches to the design of coronagraph instruments. Such instruments may include implementations of intensity masks [4], phase masks [6], phase-induced amplitude apodization [7], shaped pupils [8], visible nulling coronagraphs [9], or hybrid designs [10].

The state of the art demonstrated in the lab is summarized in Fig. A.1. Most notable amongst these results is a contrast of 2×10^{-10} with a 2% bandwidth and 2×10^{-9} with a 20% bandwidth at $3\text{--}15\lambda/D$ achieved through the use of 4th order band-limited Lyot hybrid masks [11]. Models exist that match these results, although they have not yet been formally validated. Other results plotted in Fig. A.1 are described in the follow subsections.

Hybrid Lyot Masks

John Trauger (JPL/Caltech) with a 2009 TDEM award demonstrated mean raw contrasts of 3.2×10^{-10} with a 10% bandwidth in a $284 (\lambda/D)^2$ field extending from $3\text{--}16 \lambda/D$. Raw contrasts of 1.3×10^{-9} were demonstrated with a 20% bandwidth. These results, both with unobscured pupils, are the current state of art.

The Hybrid Lyot masks that have reached $\leq 10^{-9}$ contrast performance in the HCIT are image-plane masks that appear as a linear fringe pattern of metal deposited on glass, with an additional (thus hybrid) layer of dielectric to compensate for phase errors. The throughput can be estimated from the effective pupil shear used in the mask design, which for the results reported here was a shear of 36% of the pupil thus yielding a throughput of 56% past the Lyot stop. Polarizers are not used.

Circularly symmetric masks have been fabricated for the first time as part of the WFIRST/AFTA Study and performance demonstrations with the simulated obscured pupil at the time of writing were favorable. The current limitation in performance is understood to be the ability to accurately deposit the required thickness of dielectric.

Phase-Induced Amplitude Apodization

Phase-Induced Amplitude Apodization (PIAA) is a technique for controlling diffraction that offers high throughput and small inner working angles. Apodization of pupil amplitudes is achieved by a pair of aspheric mirrors, absorbing no light aside from reflective losses. In a classic PIAA configuration, the mirrors have extreme shapes and produce a PSF with very dark sidelobes. PIAA designs have been further developed to incorporate diffraction at an occulting mask, producing the PIAA Complex Mask Coronagraph (PIAACMC), which can operate efficiently on obscured pupils. In PIAACMC under development for WFIRST/AFTA,

the mirrors have much milder shapes than the classic PIAA designs, and the occulting masks have reflective phase-only surface patterns suitable for nanofabrication.

Table A.3 Coronagraph Technology Gap List.

| ID | Title | Description | Current | Required |
|------|--|---|--|---|
| C-1 | Specialized Coronagraph Optics | Masks, apodizers, or beam-shaping optics to provide starlight suppression and planet detection capability. | A linear mask design has yielded 3.2×10^{-10} mean raw contrast from $3-16 \lambda/D$ with 10% bandwidth using an unobscured pupil in a static lab demonstration. | Circularly symmetric masks achieving $\leq 1 \times 10^{-10}$ contrast with IWA $\leq 3\lambda/D$ and $\geq 10\%$ bandwidth on obscured or segmented pupils. |
| C-2* | Low-Order Wavefront Sensing & Control | Beam jitter and slowly varying large-scale (low-order) optical aberrations may obscure the detection of an exoplanet. | Tip/tilt errors have been sensed and corrected in a stable vacuum environment with a stability of $10^{-3} \lambda$ rms at sub-Hz frequencies. | Tip/tilt, focus, astigmatism, and coma sensed and corrected simultaneously to $10^{-4} \lambda$ (~ 10 's of pm) rms to maintain raw contrasts of $\leq 1 \times 10^{-10}$ in a simulated dynamic testing environment. |
| C-3* | Large-Format Ultra-Low Noise Visible Detectors | Low-noise visible detectors for faint exoplanet characterization with an Integral Field Spectrograph. | Read noise of $< 1 e^-/\text{pixel}$ has been demonstrated with EMCCDs in a $1k \times 1k$ format with standard read-out electronics | Read noise $< 0.1 e^-/\text{pixel}$ in a $\geq 4k \times 4k$ format validated for a space radiation environment and flight-accepted electronics. |
| C-4* | Large-Format Deformable Mirrors | Maturation of deformable mirror technology toward flight readiness. | Electrostrictive 64×64 DMs have been demonstrated to meet $\leq 10^{-9}$ contrasts in a vacuum environment and 10% bandwidth. | $\geq 64 \times 64$ DMs with flight-like electronics capable of wavefront correction to $\leq 10^{-10}$ contrasts. Full environmental testing validation. |
| C-5 | Efficient Contrast Convergence | Rate at which wavefront control methods achieve 10^{-10} contrast. | Model and measurement uncertainties limit wavefront control convergence and require many tens to hundreds of iterations to get to 10^{-10} contrast from an arbitrary initial wavefront. | Wavefront control methods that enable convergence to 10^{-10} contrast ratios in fewer iterations (10-20). |
| C-6* | Post-Data Processing | Techniques are needed to characterize exoplanet spectra from residual speckle noise for typical targets. | Few 100x speckle suppression has been achieved by HST and by ground-based AO telescopes in the NIR and in contrast regimes of 10^{-5} to 10^{-6} , dominated by phase errors. | A 10-fold improvement over the raw contrast of $\sim 10^{-9}$ in the visible where amplitude errors are expected to no longer be negligible with respect to phase errors. |

*Topic being addressed by directed-technology development for the WFIRST/AFTA coronagraph. Consequently, coronagraph technologies that will be substantially advanced under the WFIRST/AFTA technology development are not eligible for TDEMs.

Classic PIAA coronagraphs have been tested at Subaru by O. Guyon, NASA Ames by R. Belikov, and JPL's HCIT by B. Kern. In 2014, JPL's HCIT completed Guyon's TDEM-09 Milestone #1, monochromatic contrast $< 1 \times 10^{-9}$, and Guyon's TDEM-10 Milestone #3, 10% broadband contrast $< 1 \times 10^{-9}$. The monochromatic milestone was met with 5×10^{-10} contrast from 2-4 λ/D , while the broadband 10% milestone was not met but achieved 1×10^{-8} from 2-4 λ/D . Also in 2014, the WFIRST/AFTA project completed its coronagraph milestone #3, which was fabrication and characterization of a PIAACMC mask meeting the WFIRST/AFTA coronagraph science requirements. The WFIRST/AFTA PIAACMC design is planned to be tested on JPL's HCIT in 2015.

The JPL HCIT laboratory demonstration of 1×10^{-8} contrast reaching a 2 λ/D working angle in 10% broadband light stands as the best demonstrated performance at small working angles (2-3 λ/D), while also exceeding 70% coronagraphic throughput. While two DMs allow a full 360-degree field-of-view, the current WFIRST/AFTA design baseline uses a single DM, located upstream of the PIAA mirrors, allowing a 180-degree field-of-view.

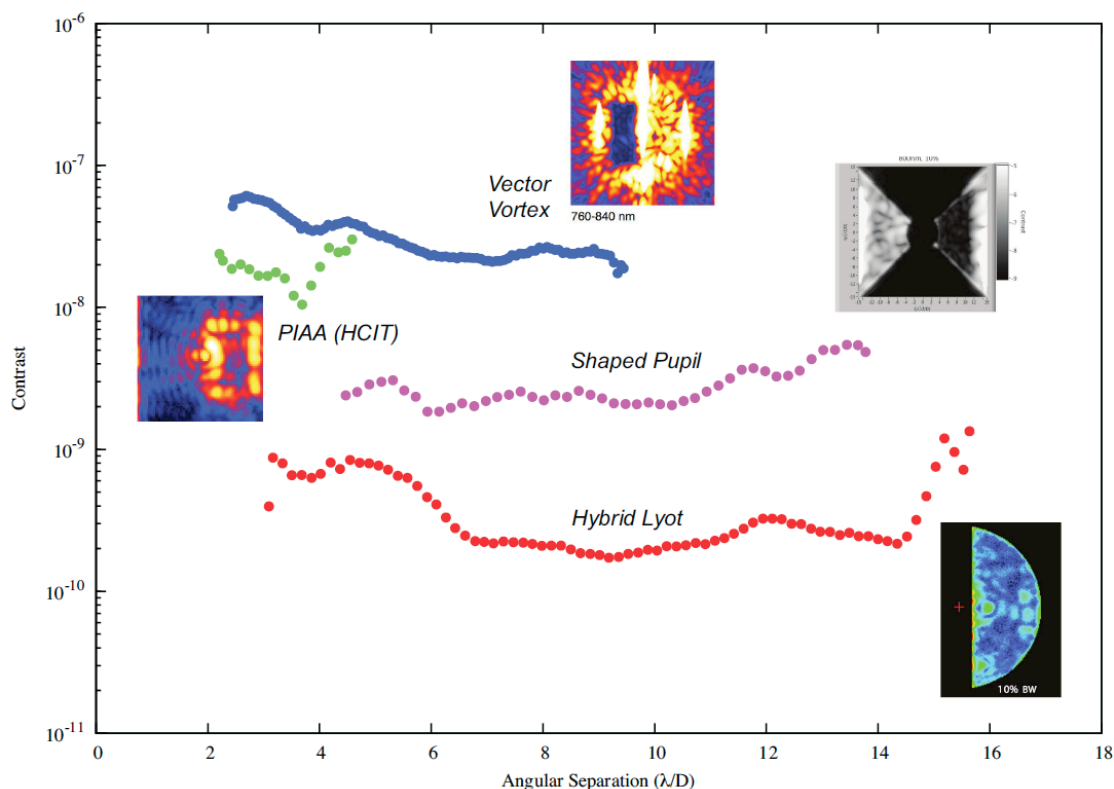


Fig. A.1: Coronagraph laboratory demonstrations using 10% bandwidth light.

Shaped Pupil Masks

A Shaped Pupil (SP) is a binary pupil-plane mask that blocks or passes light in different regions of the pupil and thus shapes the point-spread function of the coronagraph in the image plane to create dark, high-contrast regions. Because the SP coronagraph acts in a pupil plane, it is less sensitive to low-order aberrations than other coronagraphs. A field stop is usually placed at a focus between the SP and the camera to limit the dynamic range seen at the camera.

Early SP designs were optimized in 1-D for open telescope apertures and could be manufactured as free-standing, through-hole masks. New designs for obstructed telescope apertures, such as that of WFIRST/AFTA, require a 2-D optimization that produces non-freestanding opaque regions that must be placed on a substrate. Ghosting and dispersion prevent a transmissive glass substrate from being used for AFTA, so the new SPs act in reflection off a thick silicon wafer with aluminum-coated regions to reflect light and black silicon regions to absorb light. The main challenges of manufacturing reflective SPs are polishing silicon wafers to optical-quality flatness and not damaging the aluminum sections during the cryogenic etching process to create black silicon.

The first results with a reflective SP used a design for WFIRST/AFTA and one DM for wavefront correction achieved mean raw contrasts of 6×10^{-9} in 2% bandwidth light in a region from 4.4-11.2 λ/D in a 52-degree wedge. When opened to a 10% bandpass, this correction setting yielded a raw contrast of 9.1×10^{-9} . The SP used has a pupil transmission of 40% compared to the nominal obstructed aperture. No polarizers were used in these experiments.

Future designs for WFIRST/AFTA will include a diffractive focal plane mask and Lyot stop in a Shaped Pupil Lyot Coronagraph (SPLC). Such designs offer some of the robustness of a SP to low-order aberrations along with the improved performance (contrast, throughput, and/or inner working angle) of a Lyot-type coronagraph.

Vector Vortex Masks

The Vector Vortex is an image-plane mask that adjusts the phase of the incoming field, producing a rotational phase ramp of two or more even number of cycles to cancel the on-axis starlight. For the results shown here, a liquid-crystal polymer vector vortex was used.

The optical configuration is essentially identical to that of the Hybrid Lyot architecture, having only one DM for current testing, but using two for flight. No fundamental change to the mask design would be needed for flight (although material compatibility assessment in a radiation environment is still needed). The current limitation in performance is related to the ability to manufacture masks with a vortex pattern that is maintained to very small offsets from the center of rotation, and to extend the designs to broadband multi-layer masks. For the current experiments, a polarizer is required prior to the pinhole of the source.

The throughput would ideally be 100%, but the Lyot stop was undersized to 85% for the monochromatic demonstrations and to 92% for the broadband demonstrations, yielding a 72% and 85% transmission, respectively. Additionally a polarizer is used at the source (as

mentioned above), and so the effective throughput is approximately 36% monochromatic and 43% broadband.

Eugene Serabyn (JPL) with a 2010 TDEM award demonstrated mean raw contrasts of 3.2×10^{-8} with a 10% bandwidth in a $60 (\lambda/D)^2$ field extending from 2.4 – $9.4 \lambda/D$. His team later demonstrated contrast performance 4.3×10^{-10} in monochromatic light and 9×10^{-9} at 10%.

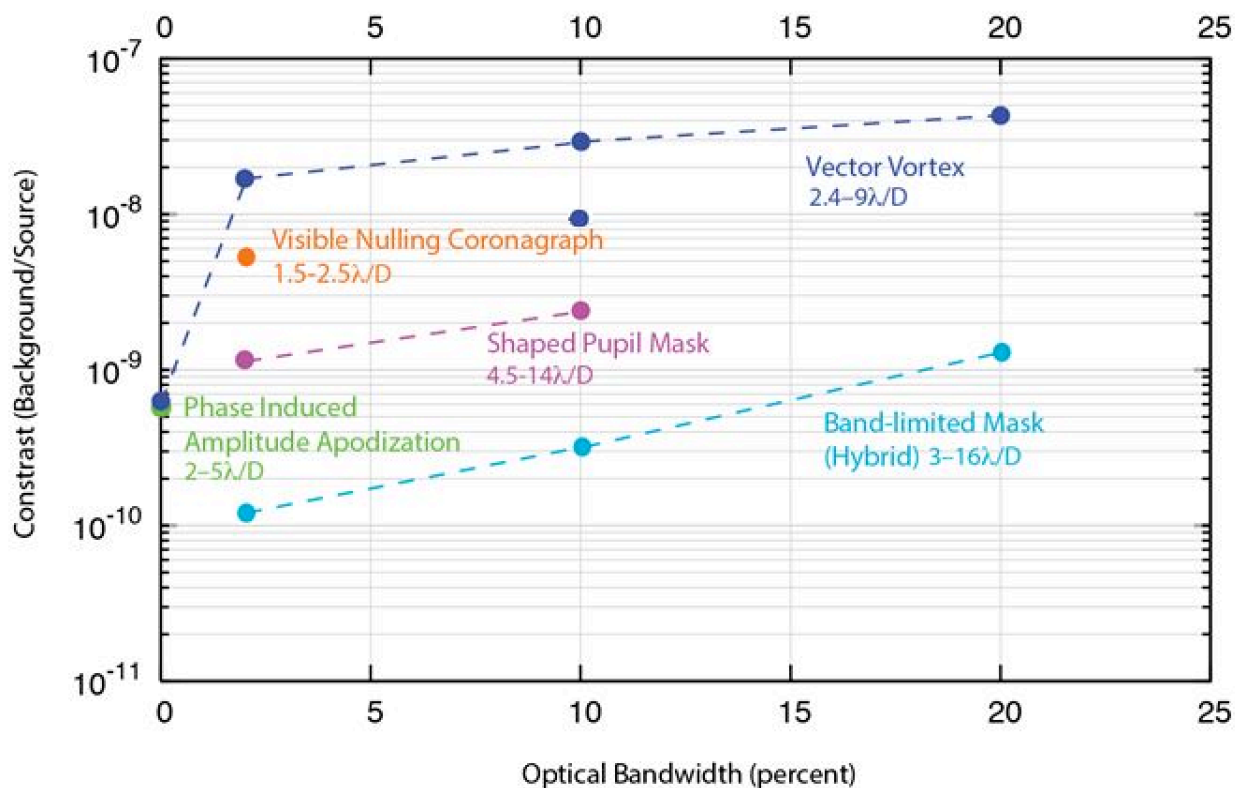


Fig. A.2: Demonstrated coronagraph contrast as a function of bandwidth. This plot summarizes results described in the text. Results reported by PIs or found in the published literature are denoted by the filled circles. Milestone results are denoted by the filled squares. The mean contrast is plotted for results that are averaged over a dark hole, i.e. averaged over an area of 4 – $10 \lambda/D$ in the case of the metallic band-limited mask. The Earth/Sun contrast at visible wavelengths would be approximately 10^{-10} .

Visible Nulling Coronagraphs

A Visible Nulling Coronagraph (VNC) uses an interferometer back-end to reject starlight via interferometric nulling with a sheared pupil. This approach uses a segmented DM with piston, tip, and tilt actuation of each segment, sometimes in combination with an array of single-mode optical fibers.

In a flight configuration, two VNC combiners would be used in series, one for each of two orthogonal image axes. The results reported here use only a single VNC combiner.

A larger outer working angle than what is possible with the 163 segment DM presently in use would be achieved using a deformable mirror with at least 300, but preferably 925

segments. The lab demonstrations used a 169 segment DM (Iris AO) and produced a wedge-shaped dark hole in the region of $2\text{--}5 \lambda/D$. Modeling will be required to determine if flight combiners would use 1) an array of single-mode fibers paired with a matched geometry DM, each having the same number of fibers and segments, respectively, or 2) two DMs. Option 1 provides spatial filtering and intensity balancing of light from each segment. The fiber array was used to demonstrate coherent imaging, but was not used for the high contrast demonstrations reported here.

If the VNC uses a single shear of 25% of the pupil, with a secondary of obscuration zero (unobscured) or 0.25, geometric throughput is 69% or 60%, respectively. A linear polarizer was used for these experiments and so the effective throughput with these aperture geometries would be approximately 35% or 30%. A new approach is anticipated for use in flight that uses both polarizations.

Mark Clampin and Rick Lyon (NASA GSFC) with their 2009 TDEM award demonstrated mean raw contrasts of 5.3×10^{-9} with a 1.2 nm wide bandpass center on 632.8 nm (0.1% bandwidth) over a $1(\lambda/D)$ circular field extending from $1.5\text{--}2.5 \lambda/D$. First broadband results (6%) are expected through their 2010 TDEM in the spring of 2015. A TDEM-13 will enable the GSFC team to use their VNC with a segmented pupil consisting of controllable mirrors to demonstrate starlight suppression for a simulated segmented mirror telescope.

A.3.2 MEMS Deformable Mirror Technology

DM development is needed in two specific areas: 1) Miniaturization of drive electronics using low-power Application-Specific Integrate Circuits (ASICs) suitable for flight. 2) A continuing program of work with DMs in 64×64 format, including operational testing of existing devices and investigation of development paths for smaller pitch and improved surface quality.

There are currently no plans to advance MEMS DMs through WFIRST/AFTA further than what is being done through the TDEM program. Two separate TDEM-10 awards were funded, to Iris AO and Boston Micromachines Corp., to continue environmental testing of both continuous face-sheet DMs as well as segmented MEMS DMs.

The goal of this effort is to better characterize their failure modes, and thus raise the TRL of the respective DM models. Paul Bierden is leading the effort on behalf of Boston Micromachines Corp; Michael Helmbrecht is leading the effort on behalf of Iris AO. Both efforts have been hampered by manufacturing issues delaying the commencement of characterization and environmental testing.

Boston Micromachines MEMS DMs, in the past, have undergone environmental testing [52] and have flown on a sounding rocket experiment [53], although in the latter case, no performance data was acquired. MEMS DMs have demonstrated a monochromatic raw contrast of 5.3×10^{-9} over angular separations of $1.5\text{--}2.5 \lambda/D$ using a Visible Nulling Coronagraph at GSFC.

A.3.3 Other Coronagraph Technologies

Efficient Coronagraph Optical Modeling

New efficient implementations of coronagraph modeling for the Vector Vortex Coronagraph (VVC), the Phase-Induced Amplitude Apodization (PIAA) coronagraph, and the Hybrid Band-Limited Coronagraph (HBLC) have been shown to be accurate to 1% or better relative to the mean field contrast for contrasts down to 10^{-10} [45] [46]. This represents a related activity because it does not include experimental validation of the models, as required in Coronagraph Milestone 3A. Models developed through this work were used to predict coronagraph performance with realistic wavefront errors [48].

This work was the subject of a 2009 TDEM award to John Krist (JPL/Caltech) and collaborators. The effort was successfully completed and two technology milestone reports were approved by the Program [45] [48]. The source code for modeling this effort is now available at <http://exep.jpl.nasa.gov/technology/>.

Model Validation of Band-limited Coronagraphs

To date no model of coronagraph performance has yet been experimentally validated, in the formal sense defined by TPF-C Milestone 3A. In 2011 initial work commenced to validate sensitivity models of band-limited coronagraphs using the same metallic mask used for TPF-C Milestone 2 [43]. Further progress was reported in 2012, 2013, and 2014 [44] [76] [77].

The effort is being continued, led by Stuart Shaklan (JPL/Caltech) and funded through a 2010 SAT-TDEM award. The TPF-C Milestone 3A Whitepaper, provides the foundation for this work [15] and is being completed in 2015.

Self-Coherent Sensing

Coronagraphs may require integration times that are many hours long, not only to detect planets but also to sense wavefront errors. Coherent speckle detection methods may provide the means to more rapidly sense and correct wavefront errors. An approach similar to the Self-Coherent Camera [49] has been demonstrated in the HCIT using a pupil-plane mask with selectable pinholes. The goal was to demonstrate the capability to measure speckles of about 1×10^{-8} contrast with uncertainty, stability, and repeatability of 20% in intensity and 1 radian in phase with 90% statistical confidence, in a window at least $2 \times 2 \lambda/D$ wide at $< 10\lambda/D$ from the star, in one spectral band of width $\geq 10\%$, with a uniform incoherent background of at least 1×10^{-8} in the area covered by the point-spread function [50]. This represents a related activity that may improve the stability of starlight-suppression experiments.

This work was conducted by Stuart Shaklan for Steven Kendrick (Ball Aerospace and Technology Corporation) and collaborators, funded through a 2009 TDEM award and successfully completed in 2012 [51].

A.4 Starshade Technology Requirements

External occulter, or starshades, block starlight by shadowing the entrance pupil of a telescope, using a physical separation between starshade and telescope sufficient to provide the necessary inner working angle. This typically requires the starshade to be tens of meters in diameter and located tens of thousands of kilometers from the telescope [54].

A starshade may have numerous petals that are each tapered to produce a desired apodization function, as seen from the telescope. The petal shapes also eliminate most edges that would otherwise both scatter and diffract starlight toward the center of the image—thus suppressing the Poisson spot that would be present if a circular occulter were used. Independent optical modeling predictions have shown excellent agreement concerning the contrast sensitivity to petal shape errors [55], and detailed preliminary error budgets have been proposed [56].

Table A.4 Starshade Technology Gap List

| ID | Title | Description | Current | Required |
|-----|---|---|--|---|
| S-1 | Control Edge-Scattered Sunlight | Limit edge-scattered sunlight with optical petal edges that also handle stowed bending strain. | Graphite edges meet all specs except sharpness, with edge radius $\geq 10 \mu\text{m}$. | Optical petal edges manufactured of high flexural strength material with edge radius $\leq 1 \mu\text{m}$ and reflectivity $\lesssim 10\%$. |
| S-2 | Contrast Performance Demonstration and Optical Model Validation | Experimentally validate the equations that predict the contrasts achievable with a starshade. | Experiments have validated optical diffraction models at Fresnel number of ~ 500 to contrasts of 3×10^{-10} at 632 nm. | Experimentally validate models of starlight suppression to $\leq 3 \times 10^{-11}$ at Fresnel numbers ≤ 50 over 510-825 nm bandpass. |
| S-3 | Lateral Formation Flying Sensing Accuracy | Demonstrate lateral formation flying sensing accuracy consistent with keeping telescope in starshade's dark shadow. | Centroid accuracy $\geq 1\%$ is common. Simulations have shown that sensing and GN&C is tractable, though sensing demonstration of lateral control has not yet been performed. | Demonstrate sensing lateral errors $\leq 0.20\text{m}$ at scaled flight separations and estimated centroid positions $\leq 0.3\%$ of optical resolution. Control algorithms demonstrated with lateral control errors $\leq 1\text{m}$. |
| S-4 | Flight-Like Petal Fabrication and Deployment | Demonstrate a high-fidelity, flight-like starshade petal and its unfurling mechanism. | Prototype petal that meets optical edge position tolerances has been demonstrated. | Demonstrate a fully integrated petal, including blankets, edges, and deployment control interfaces. Demonstrate a flight-like unfurling mechanism. |
| S-5 | Inner Disk Deployment | Demonstrate that a starshade can be autonomously deployed to within the budgeted tolerances. | Demonstrated deployment tolerances with 12m heritage Astromesh antenna with four petals, no blankets, no outrigger struts, and no launch restraint. | Demonstrate deployment tolerances with flight-like, minimum half-scale inner disk, with simulated petals, blankets, and interfaces to launch restraint. |

Two similar approaches to the design of external occulter have been studied, differing by whether an analytical petal shape is used [57][58] or whether it derives from a mathematical optimization [59][60]. Several different implementations are being investigated for the packaging and deployment of a starshade: one example is the use of deployable booms [61][62]; another is the use of an unfurling truss [63][64].

The subject areas for starshade milestones are described in the sections below and summarized in Table A.4. Milestone topics are related to the materials, design, fabrication, and predicted optical performance of the as-built components and subsystems. Other milestones cover topics that must be demonstrated at the system level and include deployment, dynamic behavior, as well as guidance, navigation, and control. The results of the starshade technology development tasks must demonstrate that the on-orbit performance is achievable based upon a well-grounded understanding of the error budget, backed by the necessary laboratory results.

A.4.1 Control of Scattered Sunlight

Small amount of sunlight reflects and diffracts from the starshade optical edge into the telescope, appearing as solar glint and contributes to instrument background noise. A system model was developed to predict solar glint fluxes as a function of solar incidence angle and validated by testing a variety of representative edges in a scatterometer testbed. Progress in this area has been reported by Stefan Martin (JPL/Caltech) and collaborators [72].

Currently active engineering tasks are evaluating various materials with the requisite reflectivity that are also compatible with the petal structure for thermal deformations, bending strain from stowed to full deployment, and handling safety requirements.

Research in this area is being conducted through a TDEM-12 award to Suzi Casement (Northrop Grumman) and a JPL RT&D award.

A.4.2 Validation of Starshade Optical Models

Starshade optical performance will not be demonstrated by ground-based testing of any full-scale unit due to the requisite distances being prohibitive. Rather, it will be demonstrated in a two-step process. First, subscale tests will demonstrate contrast performance consistent with imaging exo-Earths and validate the optical models, upon which full-scale shape tolerance allocations are based. The scaling approach is to match the flight design in terms of the number of Fresnel zones across the starshade, such that the diffraction equations defining the dark shadow are identical.

Second, shape tolerance allocations will be verified on the fully deployed flight unit. Key capabilities are already demonstrated via early prototypes.

Several experiments over the last decade demonstrate the viability of creating a dark shadow with a starshade, including: the University of Colorado [66] [78]; Northrop-Grumman [68]; Princeton University [79]; [67]; and larger scale tests in a dry lake-bed [73]. Each of these experiments is limited in contrast performance to some extent by a subset of the following test environment issues:

- Wavefront errors due to collimating optics
- Dust in open air testing
- Diffraction effects due to the finite extent of the optical enclosure

- Diffraction off starshade support struts

The current starshade optical testbed at Princeton University addresses the limitations identified above to yield the darkest shadow produced by a starshade to date. An expanding beam is used to eliminate collimating optics and accounts for the corresponding contribution to Fresnel number. It also helps to limit testbed length to a manageable level. Dust effects are limited by testing in an indoor facility within an optical enclosure. Diffraction effects from the optical enclosure and support struts are mitigated with an innovative mounting scheme whereby the starshade is supported by an outer ring with an apodization profile optimized in similar fashion to the starshade profile. This introduces a non-flight outer working angle (OWA) limit at the tip of the outer ring.

A new TDEM activity (TDEM-12) led by Professor N. Jeremy Kasdin of Princeton University is underway to address optical performance verification and model validation. The development and testing of an improved subscale starshade with optical edge thickness $\leq 1 \mu\text{m}$ is their first priority. This is expected to greatly reduce starlight glint. An effort to model the observed glint is also planned. A completely new and much improved optical testbed is planned with length greater than 50 m. The goal is to achieve a Fresnel number approaching a flight design. The starlight simulator will also be capable of producing broadband light.

A separate TDEM-12 activity led by Tiffany Glassman of NGAS is also underway to improve upon the open air testing of 60 cm starshades. Test objectives include demonstrating contrast better than 10^{-9} at all radii outside of the starshade tips and demonstrating agreement between the measured and predicted contrasts when testing starshade masks with intentional fabrication errors.

A.4.3 Lateral Formation Flying Sensing Accuracy

The starshade is designed to produce a dark shadow that extends radially 1 m beyond the telescope aperture. Contrast degrades rapidly beyond the 1 m specification. Formation control is required to keep the starshade center positioned laterally within ± 1 m of the telescope boresight. This requires sensing the lateral position error to within 30 cm. The axial separation distance between starshade and telescope is loosely controlled to within ± 250 km. Formation flying control is straightforward because of a very benign disturbance environment. The control system simply has to keep the telescope within the dark-shadow created by the starshade. A specific aspect of the problem to qualify as an “unresolved technology issue” is formation sensing. Starshade lateral position must be sensed with 3-sigma accuracy better than ± 30 cm, relative to the telescope bore-sight, which is pointed at the target star.

Two factors make the formation sensing challenge tractable. First, the formation sensor utilizes the relatively large science telescope. It simultaneously images both the starshade laser beacon and the target star, as indicated by long, out-of-band wavelengths that diffract into the shadow. Onboard image processing algorithms must estimate centroid positions with 3-sigma accuracy better than 0.3% of optical resolution. Built into these algorithms is a model of starshade diffraction at long wavelengths. Second, the environment is very benign in Earth-leading orbit. Solar pressure is the dominant disturbance and yields a very low control bandwidth. This contributes to improving formation-sensing accuracy with long sensor integration times.

Two TDEM-13 tasks starting in 2015 have been awarded to demonstrate the requisite formation flying sensors capability. Jeremy Kasdin of Princeton University leads the development of a breadboard instrument, including Formation Guidance Channel (FGC) and image processing algorithms, which will be integrated into the Princeton starshade optical testbed. The detector will be mounted on a two-axis stage to simulate lateral position errors. This TDEM will also develop the system design for formation flying and prototype algorithms for formation sensing, in addition to trajectory estimator and formation control algorithms. Early simulations will demonstrate performance and assist in exploring optimal formation control and acquisition strategies, in terms of fuel usage. After integrating the instrument breadboard into the starshade optical testbed the control loop will be demonstrated with detector position stages simulating thrusters.

Webster Cash of the University of Colorado, Boulder leads the development of two wavefront sensors that will advance long distance formation flying sensing. The proposed experiments will demonstrate medium and fine level alignment sensors that have been previously identified as potential formation flying sensors for external occulter. The medium level sensor is an astrometric telescope located on the starshade that guides the starshade as it slews between stars and up to the onset of the shadow onto the science telescope. Once in the shadow, a wavefront sensor on the science telescope uses long wavelength starlight diffracted around the starshade (a phenomenon known as the spot of Arago) to map the distribution of light at the aperture and to guide to the center of the shadow. Recovered intensity from behind the starshade of $> 1\%$ at wavelengths outside of the science bandpass will be measured, and the measured wavefronts at different wavelengths and starshade configurations will be used to validate model predictions. This will be the first demonstration of starshades at wavelengths $> 1 \mu\text{m}$ and will provide a new wavelength regime in which to investigate the starshade's performance and validate the state of the art diffraction codes.

A.4.4 Flight-Like Petal Fabrication and Deployment

An initial challenge of constructing a starshade is to demonstrate that the mechanical tolerances for a petal can be met, as derived from a complete starshade error budget. The petal width profile must be manufactured to within a tolerance of $\pm 100 \mu\text{m}$. Compliance was demonstrated by test through a TDEM activity (TDEM-09) led by Jeremy Kasdin of Princeton University. Prior work at NGAS demonstrated that precision petal tips and valleys are also manufacturable to the required tolerances [69].

Princeton University TDEM-09 results fully demonstrated the achievability of the allocated manufacturing tolerances on petal width profile. However, the flight build will benefit from investment in an *in-situ metrology tool*. This tool will be mated to the assembly table (i.e., optical bench) and used for petal assembly, edge installation, and final shape measurement without moving the petal. Improvement is also available in the optical edge machining accuracy, relative to the conventional CNC router used for this TDEM. A simplification for this TDEM is the use of square-cut optical edge segments. The flight unit requires a sharp bevel cut edge to limit scattered sunlight. This may change the type of metrology sensor head, but does not invalidate the results.

A new TDEM activity (TDEM-12) led by Jeremy Kasdin of Princeton University is underway to retire the petal manufacturability risk by building a petal at full-scale with flight-like

materials with sharp bevel cut edges. Flight-like materials are equivalent to flight materials without the expensive material certifications. This petal will demonstrate deployment from stow to full deployment position with measurements that show compliance with the allocated tolerance. Other tests to demonstrate the petal robustness in thermal and launch vibration environments are currently being evaluated and prioritized based on limited funding.

A solution for petal unfurling is currently being examined by an SBIR company called Roccor in collaboration with JPL.

A.4.5 Inner Disk Deployment

Each petal attaches to the inner disk at two hinge points and the deployed position of these hinge points must be precisely controlled. The diameter of the best-fit circle through all petal hinge points represents the achieved inner disk diameter, and the allocated tolerance (i.e., mean radial bias error) is ± 0.25 mm. The allocated random tolerance is ± 0.5 mm in each of radial and tangential directions. There is no tangential mean position bias.

Compliance was demonstrated through a TDEM-10 activity led by Jeremy Kasdin of Princeton University. After ten initial deployment/metrology cycles, mechanical shims were installed to reduce the mean radial bias error. An additional 15 deployment cycles were measured for the final data set. The results showed 90% confidence level with 3-sigma uncertainty that all perimeter truss positions are contained within the allocated tolerance.

A new Starshade Deployment Testbed (SDT) was completed in 2014 that integrated starshade upgrades to the perimeter truss design (Figure A.3). This testbed was fabricated at half-scale and currently serves as the testbed to improve the precision control of the perimeter truss and for demonstrating other technologies such as the optical shields for the inner disk structure.

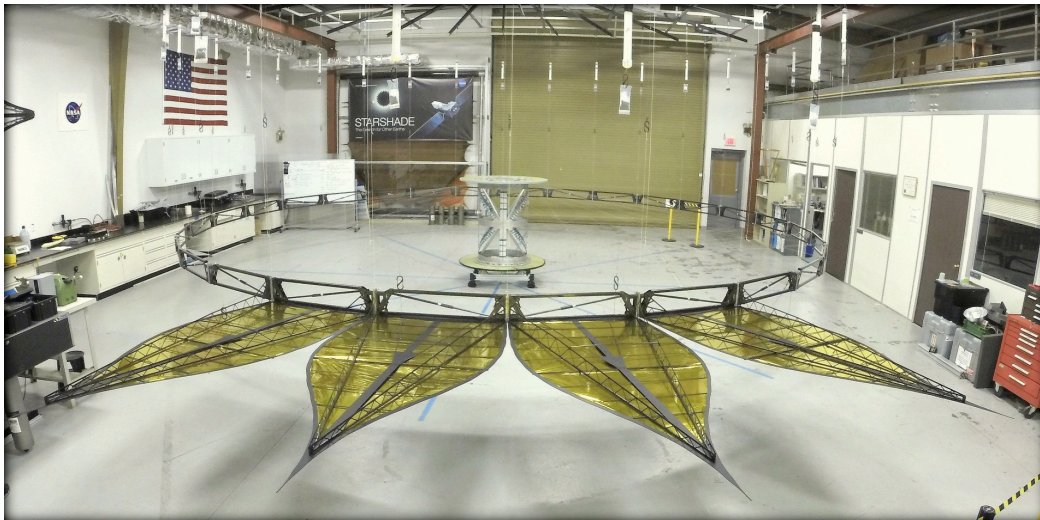


Figure A.3: Starshade Deployment Testbed at JPL has 10 m diameter perimeter truss with gravity compensation fixtures for the truss and the petals. Principal Investigators are welcome to use this testbed to advance Starshade technology gaps.

A.4.6 Other Starshade Technologies

Thermal Deformations

Early contrast error budget estimates identified starshade thermal deformation as a potentially significant contributor. Subsequent analyses have shown that through careful material selection the expected thermal deformations can be easily kept within budgeted tolerances. As such, thermal deformation management is viewed as a routine engineering development effort and not technology development. Margins are deemed sufficiently large to defer test-based verification. However, tests are being evaluated to validate thermal deformations and prioritized based on limited funding.

Holes and Opacity

Since the starshade covers significant area and is largely constructed of the thin, light-weight optical shield (OS), it is susceptible to holes created by micrometeoroids. A cumulative pinhole area of 1 cm² introduces a contrast contribution of 1×10^{-12} . Modeling of this current OS design and known micrometeoroid fluxes show the design to be conservative.

Leveraging relevant knowledge from the James Webb Space Telescope development for micrometeoroid protection will be essential. Tests to demonstrate robustness against micrometeoroid impact are being evaluated and prioritized based on limited funding. The current technology development plan is to evaluate micrometeoroids by modeling only.

A.5 Conclusion

The 2010 Astrophysics Decadal Survey recommended the creation of a technology development program for a potential future exoplanet mission to mature starlight-suppression technology for the detection of spectra of Earth-like exoplanets. The ExEP supports a community-based process to help NASA identify the needed technologies to achieve this goal and to mature the selected concepts so to inform the 2020 Decadal Survey committee. This Appendix outlines technology development that will lead toward that goal.

A new Technology Plan Appendix will be released each year to update the progress made in each technology area and to identify new SAT-TDEM opportunities.

A.6 Bibliography

- [1] NRC Astronomy and Astrophysics Survey Committee, *New Worlds, New Horizons in Astronomy and Astrophysics*, 2010, The National Academies Press, Washington, DC, 2010.
- [2] Traub, W. A. & Oppenheimer, B. R. 2010, "Direct Imaging of Exoplanets," in *Exoplanets*, Seager, S., ed., University of Arizona Press, pp. 111–156.
- [3] Mawet, D., Pueyo, L., Lawson, P., et al. 2012, "Review of small-angle coronagraphic techniques in the wake of ground-based second-generation adaptive optics systems," *Proc. SPIE* 8442, 844204.
- [4] Lawson, P. R., Belikov, R., Cash, W., et al. 2013, "Survey of experimental results in high-contrast imaging for future exoplanet missions," *Proc. SPIE* 8864, 88641F.
- [5] Trauger, J. T., & Traub, W. A. 2007, "A laboratory demonstration of the capability to image an Earth-like extrasolar planet," *Nature* 446, pp. 771–773.
- [6] Mawet, D., Serabyn, E., Liewer, K., et al. 2009, "Optical Vectorial Vortex Coronagraphs using Liquid Crystal Polymers: theory, manufacturing and laboratory demonstration," *Optics Express* 17, pp. 1902–1918.
- [7] Guyon, O. 2003, "Phase-induced amplitude apodization of telescope pupils for extrasolar terrestrial planet imaging," *Astron. Astrophys.* 404, pp. 379–387.
- [8] Kasdin, N. J., Carlotti, A., Pueyo, L., Groff, T., Vanderbei, R. 2011, "Unified coronagraph and wavefront control design," *Proc. SPIE* 8151, 81510Y
- [9] Lyon, R. G., Clampin, M., Woodruff, R. A., et al. 2010, "Visible nulling coronagraphy testbed development for exoplanet detection," *Proc. SPIE* 7731.
- [10] Moody, D. C., Gordon, B. L., & Trauger, J. T. 2008, "Design and demonstration of hybrid Lyot coronagraph masks for improved spectral bandwidth and throughput," *Proc. SPIE* 7010.
- [11] Trauger, J., Moody, D., Gordon, B., Krist, J., Mawet, D. 2011, "A hybrid Lyot Coronagraph for the direct imaging and spectroscopy of exoplanet systems," *Proc. SPIE* 8151, 81510G.
- [12] Kern, B., Kuhnert, A., & Trauger, J. 2008, eds., *Exoplanet Exploration Technology Milestone #2 Report*, Jet Propulsion Laboratory Publications, Pasadena, California, JPL Document 60951.
- [13] Trauger, J., Stapelfeldt, K., Traub, W., et al. 2010, "ACCESS: a concept study for the direct imaging and spectroscopy of exoplanetary systems," *Proc. SPIE* 7731, pp. 773128–+.
- [14] Trauger, T., Kern, B., & Kuhnert A., eds., 2006, *TPF-C Technology Milestone #1 Report*, Jet Propulsion Laboratory Publications, Pasadena, California, JPL Document 35484.

- [15] Shaklan, S., 2009, Exoplanet Exploration Coronagraph Technology Milestone #3A White Paper: Coronagraph Stalight Suppression Model Validation, Jet Propulsion Laboratory Publications, Pasadena, California, JPL Document 64582.
- [16] Soummer, R., Pueyo, L., Ferrari, A., et al. 2009, "Apodized pupil Lyot coronagraphs for arbitrary apertures. II. Theoretical properties and application to extremely large telescopes," *Astrophys. J.* 695, 695-706.
- [17] Mawet, D., Serabyn, E., Wallace, J. K., & Pueyo, L. 2011, "Improved high-contrast imaging with on-axis telescopes using a multistage vortex coronagraph," *Opt. Lett.* 36, 1506-1508.
- [18] Guyon, O., Kern, B., Belikov, R., et al. 2012, "Phase Induced Amplitude Apodization (PIAA) coronagraphy: Recent results and future prospects," *Proc. SPIE* 8442, 84424V.
- [19] Carlotti, A., Kasdin, N. J., Vanderbei, R. J., Delorme, J.-R. 2012, "Optimized shaped pupil masks for pupil with obscuration," *Proc. SPIE* 8442, 844254.
- [20] Riggs, A. J. E., Groff, T. D., Carlotti, A., et al. 2013, "Demonstration of symmetric dark holes using two deformable mirrors at the high-contrast imaging testbed," *Proc. SPIE* 8864, 88640T.
- [21] Trauger, J., Gordon, B., Krist, J. et al. 2010, "Technology Milestone Whitepaper: Hybrid Lyot Coronagraph Technology – Linear Masks," Jet Propulsion Laboratory Doc. D-64843. <http://exep.jpl.nasa.gov/technology>.
- [22] Trauger, J., Moody, D., Gordon, B., Krist, J., and Mawet, D. 2012, "Complex apodization Lyot coronagraphy for the direct imaging of exoplanet systems: design, fabrication, and laboratory demonstration," *Proc. SPIE* 8442, 84424Q.
- [23] Belikov, R., Pluzhnik, Witteborn, F. C., et al. 2011, "Laboratory demonstration of high-contrast imaging at inner working angles better than $2 \lambda/D$ and better," *Proc. SPIE* 8151, 815102.
- [24] Kern, B., Guyon, O., Give'on, A., Kuhnert, A., Niessner, A. 2011, "Laboratory testing of a Phase-Induced Amplitude Apodization (PIAA) coronagraph," *Proc. SPIE* 8151, 815104.
- [25] Guyon, O., Schneider, G., Close, L. et al. 2010, "Technology Milestone Whitepaper: Phase-Induced Amplitude Apodization Coronagraph: Monochromatic Contrast Demonstration," Jet Propulsion Laboratory Doc. D-65830. <http://exep.jpl.nasa.gov/technology>.
- [26] Guyon, O., Schneider, G., Close, L., et al. 2011, "Technology Milestone #2 Whitepaper: Instrument Tip-Tilt Control Demonstration at the sub-Milliarcsecond Level," Jet Propulsion Laboratory Doc. D-71066. <http://exep.jpl.nasa.gov/technology>.
- [27] Guyon, O., Kern, B., Belikov, R., et al. 2012, "Phase Induced Amplitude Apodization (PIAA) coronagraphy: Recent results and future prospects," *Proc. SPIE* 8442, 84424V.
- [28] Kern, B. D., Guyon, O., Kuhnert, A., et al. 2013, "Laboratory demonstration of Phase Induced Amplitude Apodization (PIAA) coronagraph with better than 10^{-9} contrast," *Proc. SPIE* 8864, 88640R.

- [29] Sidick, E., Kern, B., Kuhnert, A., et al. 2013, "Comparisons of simulated contrast performance of different Phase Induced Amplitude Apodization (PIAA) coronagraph configurations," Proc. SPIE 8864, 88641Y.
- [30] Mawet, D. P., Serabyn, E., Moody, D., et al. 2011, "Recent results of the second generation of vector vortex coronagraphs on the High Contrast Imaging Testbed at JPL," Proc. SPIE 8151, 81511D.
- [31] Serabyn, E., Mawet, D., Burruss, R. 2010, "An image of an exoplanet separated by two diffraction beamwidths from a star," Nature 464, 1018.
- [32] Mawet, D., Serabyn, E., Wallace, J. K., et al. 2011, "Improved high-contrast imaging with on-axis telescopes using a multistage vortex coronagraph," Opt. Lett. 36, 1506.
- [33] Serabyn, G., Krist, J., Mawet, D., Moody, D., and Trauger, J. 2012, "Technology Milestone Whitepaper: Vortex Coronagraph Technology," Jet Propulsion Laboratory Doc. D-73329. <http://exep.jpl.nasa.gov/technology>.
- [34] Serabyn, E., Trauger, J. T., Moody, D., et al. 2013, "High-contrast imaging results with the vortex coronagraph," Proc. SPIE 8864, 88640Y.
- [35] Stewart, J. B., Bifano, T. G., Cornelissen, S., Bierden, P., Levine, B. M., Cook, T. 2007, "Design and development of a 331-segment tip-tilt-piston mirror array for space-based adaptive optics," Sensors and Actuators A 138, 230-238.
- [36] Helmbrecht, M. A., He, M., Kempf, C. J. 2012, "Development of high-order segmented MEMS deformable mirrors," Proc. SPIE 8253, 825307.
- [37] Lyon, R. G., Clampin, M., Petrone, P., Mallik, U., Madison, T., and Bolcar, M. R. 2012, "High contrast Vacuum Nuller Testbed (VNT) contrast, performance and null control," Proc. SPIE 8442, 844208.
- [38] Lyon, R. G., Clampin, M., Petrone, P., et al. 2011, "Vacuum nuller testbed (VNT) performance, characterization and null control: progress report," Proc. SPIE 8151, 81510G.
- [39] Clampin, M. 2011, "Technology Milestone #1 Whitepaper: Visible Nulling Coronagraph Technology Maturation: High Contrast Imaging and Characterization of Exoplanets," Jet Propulsion Laboratory Doc. D-68671. <http://exep.jpl.nasa.gov/technology>.
- [40] Belikov, R., Give'on, A., Kern, B., et al. 2007, "Demonstration of high contrast in 10% broadband light with the shaped pupil coronagraph," Proc. SPIE 6693.
- [41] Pueyo, L., Kay, J., Kasdin, N. J., et al. 2009, "Optimal dark hole generation via two deformable mirrors with stroke minimization," Appl. Opt. 48, pp. 6296-6312.
- [42] Groff, T. D., Kasdin, N. J., Carlotti, A., and Eldorado Riggs, A. J. 2012, "Broadband focal plane wavefront control of amplitude and phase aberrations," Proc. SPIE 8442, 84420C.
- [43] Sidick, E., Shaklan, S., Give'on, A., Kern, B. 2011, "Studies of the effects of optical system errors on the HCIT contrast performance," Proc. SPIE 8151, 815106.
- [44] Sidick, E., Shaklan, S., Balasubramanian, K. 2012, "HCIT broadband contrast performance sensitivity studies," Proc. SPIE 8520, 85200M.

- [45] Krist, J., Belikov, R., Mawet D. et al. 2012, "Technology Milestone #1 Report: Assessing the performance limits of internal coronagraphs through end-to-end modelling," Jet Propulsion Laboratory Doc. D-74425. <http://exep.jpl.nasa.gov/technology>.
- [46] Krist, J. E., Belikov, R., Pueyo, L., et al. 2011, "Assessing the performance limits of internal coronagraphs through end-to-end modelling: a NASA TDEM study," Proc. SPIE 8151, 81510E.
- [47] Krist, J. E., Belikov, R., Pueyo, L., et al. 2011, "Assessing the performance limits of internal coronagraphs through end-to-end modelling," Proc. SPIE 8864, 88640P.
- [48] Krist, J., Belikov, R., Mawet D. et al. 2012, "Technology Milestone #2 Report: Assessing the performance limits of internal coronagraphs through end-to-end modelling," Jet Propulsion Laboratory Doc. D-74426. <http://exep.jpl.nasa.gov/technology>.
- [49] Galicher, R., Baudoz, P., Rousset, G., et al. 2010, "Self-coherent camera as a focal plane wavefront sensor: simulations," A&A 509, A.31.
- [50] Give'on, A., Shaklan, S., Kern, B., Noecker, C., Kendrick, S., and Wallace, K. 2012, "Electric field reconstruction in the image plane of a high-contrast coronagraph using a set of pinholes around the Lyot plane," Proc. SPIE 8442, 84420B.
- [51] Shaklan, S., Kern, B., Give'on, A., et al. 2012, "Technology Milestone Report: Advancing Speckle Sensing for Internal Coronagraphs," Jet Propulsion Laboratory Document D-73509. <http://exep.jpl.nasa.gov/technology>.
- [52] Enya, K., Abe, L., Takeuchi, S., et al., 2011, "A high dynamic-range instrument for SPICA for coronagraphic observation of exoplanets and monitoring of transiting exoplanets," Proc. SPIE 8146, 81460Q.
- [53] Mendillo, C. B., Hicks, B. A., Cook, T. A., et al. 2012, "PICTURE: a sounding rocket experiment for direct imaging of an extrasolar planetary environment," Proc. SPIE 8442, 84420E.
- [54] Turnbull, M. C., Glassman, T., Roberge, A., et al. 2012, "The search for habitable worlds. 1: The viability of a starshade mission," Pub. Astron. Soc. Pac. 124, 418-447.
- [55] Shaklan, S. B., Noecker, M. C., Glassman, T., et al. 2010, "Error budgeting and tolerancing of starshades for exoplanet detection," Proc. SPIE 7731, 77312G.
- [56] Shaklan, S. B., Marchen, L., Lisman, P. D., et al. 2011, "A starshade petal error budget for exo-earth detection and characterization," Proc. SPIE 8151, 815113.
- [57] Copi, C. J., and Starkman, G. D. 2000, "The Big Occulting Steerable Satellite (BOSS)," Astrophys. J. 532, 581-592.
- [58] Cash, W. 2006, "Detection of Earth-like planets around nearby stars using a petal-shaped occulter," Nature 442, pp. 51-53.
- [59] Vanderbei, R. J., Cady, E., & Kasdin, N. J. 2007, "Optimal Occulter Design for Finding Extrasolar Planets," Astrophys. J. 665, pp. 794-798.
- [60] Cady, E. 2011, "Nondimensional representations for occulter design and performance evaluation," Proc. SPIE 8151, 815112.

- [61] Lo, A., Cash, W., Hyde, T., Polidan, R., & Glassman, T. 2009, "Starshade Technology Development: Astro2010 Technology Development Whitepaper," ArXiv Astrophysics e-prints 2010, pp. 44-+.
- [62] Cash, W., Kendrick, S., Noecker, et al., 2009, "The New Worlds Observer: the astrophysics strategic mission concept study," Proc. SPIE 7436.
- [63] Thomson, M. W., Lisman, P. D., Helms, R., et al. 2010, "Starshade design for occulter based exoplanet missions," SPIE 7731.
- [64] Kasdin, N. J., Spergel, D. N., Lisman, D., et al. 2011, "Advancing technology for starlight suppression via an external occulter," Proc. SPIE 8151, 81510J.
- [65] Kasdin, N. J., Lisman, D., Shaklan, S., et al. 2013, "Verifying occulter deployment tolerances as part of NASA's technology development for exoplanet missions," Proc. SPIE 8864, 886417.
- [66] Schindhelm, E., Shipley, A., Oakley, P., et al. 2007, "Laboratory studies of petal-shaped occulter" Proc. SPIE 6693, 669305.
- [67] Sirbu, D., Kasdin, N. J., Vanderbei, R. J., 2013, "Progress on optical verification for occulter-based high contrast imaging," Proc. SPIE 8864, 886419.
- [68] Samuele, R., Varshneya, R., Johnson, T. P., et al. 2010, "Progress at the starshade testbed at Northrop Grumman Aerospace Systems: comparisons with computer simulations," Proc. SPIE 7731.
- [69] Lo, A. S., Glassman, T., Dailey, D., Sterk, K., Green, J., Cash, W., Soummer, R. 2010, "New Worlds Probe," Proc. SPIE 7731, 77312E.
- [70] Kasdin, N. J., Lisman, D., Shaklan, S., et al. 2012, "Technology demonstration of starshade manufacturing for NASA's Exoplanet Mission Program," Proc. SPIE 8442, 84420A.
- [71] Kasdin, N. J., Spergel, D. N., Vanderbei, R., et al. 2012, "Technology Milestone Report: Advancing Technology for Starlight Suppression via an External Occulter," Jet Propulsion Laboratory Document D-74384. <http://exep.jpl.nasa.gov/technology>.
- [72] Martin, S. R., Shaklan, S. B., Crawford, S. L., et al. 2013, "Starshade optical edge modelling, requirements, and laboratory tests," Proc. SPIE 8864, 88641A.
- [73] Glassman, T., Casement, S., Warwick, S., et al. 2013, "Achieving high-contrast ratios with a 60-cm starshade," Proc. SPIE 8864, 886418.
- [74] Figer, D. 2010, "Technology Milestone Whitepaper: A Photon-Counting Detector for Exoplanet Missions," Jet Propulsion Laboratory. D-93392. <http://exep.jpl.nasa.gov/technology>.
- [75] Figer, D., Lee, J., Hanold, B. J., et al. 2011, "A photon-counting detector for exoplanet missions," Proc. SPIE 8151, 81510K.
- [76] Sidick, E., Shaklan, S., Krist, J., Cady, E., Kern, B., and Balasubramanian, K. 2013 "HCIT contrast performance sensitivity studies: simulation vs. experiment," Proc. SPIE 8864, 88640Q

- [77] Sidick, E., Shaklan, S., Balasubramanian, K., and Cady, E. 2014, "High-contrast coronagraph performance in the presence of focal plane mask defects," Proc. SPIE 9143, 914336.
- [78] Leviton, D. B., Cash, W. C., Gleason, B., et al. 2007, "White-light demonstration of one hundred parts per billion irradiance suppression in air by new starshade occulter." Proc. SPIE 6687.
- [79] Cady, E., Balasubramanian, K., Dickie, M., et al. 2009, "Progress on the occulter experiment at Princeton." Proc. SPIE 7440, 744006.